ARTICLE

Ion-Velocity Map Imaging Study of Photodissociation Dynamics of Acetaldehyde

Zhi-guo Zhang[a,b], Zhi-chao Chen[b], Cui-mei Zhang[a,b], Yan-ling Jin[b], Qun Zhang[a*], Yang Chen[a*], Cun-shun Huang[b*], Xue-ming Yang[a,b]

a. Hefei National Laboratory for Physical Sciences at the Microscale and Department of Chemical Physics, University of Science and Technology of China, Hefei 230026, China
b. State Key Laboratory of Molecular Reaction Dynamics, Dalian Institute of Chemical Physics, Dalian 116023, China

(Dated: Received on February 19, 2014; Accepted on April 11, 2014)

The photodissociation dynamics of acetaldehyde in the radical channel CH_3+HCO has been reinvestigated using time-sliced velocity map imaging technique in the photolysis wavelength range of 275−321 nm. The CH_3 fragments have been probed via (2+1) resonance-enhanced multiphoton ionization. Images are measured for CH_3 formed in the ground and excited states (v_2=0 and 1) of the umbrella vibrational mode. For acetaldehyde dissociation on T_1 state after intersystem crossing from S_1 state, the products are formed with high translational energy release and low internal excitation. The rotational and vibrational energy of both fragments increases with increasing photodissociation energy. The triplet barrier height is estimated at 3.881±0.006 eV above the ground state of acetaldehyde.

Key words: Ion-velocity map imaging, Photodissociation dynamics, Acetaldehyde

I. INTRODUCTION

Acetaldehyde (CH_3CHO) plays a significant role in both clean and polluted atmospheres due to its participation in the ozone formation or in the oxidation of volatile pollutants compounds. It is one of the typical carbonyl compounds whose photochemistry and spectroscopy have been extensively studied for many years both experimentally [1−22] and theoretically [23−37]. The main feature in the acetaldehyde absorption spectrum is located in the wavelength range between 250 and 350 nm, which corresponds to the transition to the singlet state (S_1) from the ground singlet state (S_0). The potential energy surfaces of the three lowest electronic states of acetaldehyde are shown in Fig.1. After excitation to the S_1 state, acetaldehyde is deactivated by fluorescence emission or internal conversion to highly vibrationally excited state of S_0. The S_1-state acetaldehyde also dissociates into the fragments by intersystem crosses to the triplet state T_1 or internal conversion to S_0.

The photodissociation dynamics of CH_3CHO on the singlet state (S_1) is complicated by the participation of three potential energy surfaces (PESs), S_0, S_1, and T_1. The following several dissociation channels are energetically accessible after excitation within the S_1←S_0 absorption region:

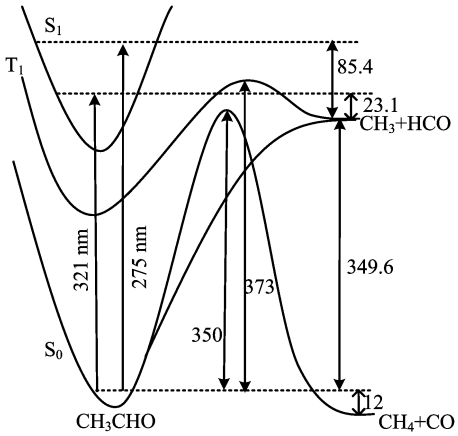

FIG. 1 Schematic potential energy diagram for the three lowest electronic states of acetaldehyde. The vertical arrows indicate the photodissociation energy at 275 and 321 nm. Energies are reported in kJ/mol with zero point energies included (from Ref.[18]).

$$CH_3CHO(S_0) + h\nu \rightarrow CH_3CO + H \quad (1)$$
$$CH_3CHO(S_0) + h\nu \rightarrow CH_2CHO + H \quad (2)$$
$$CH_3CHO(S_0) + h\nu \rightarrow CH_2CO + H_2 \quad (3)$$
$$CH_3CHO(S_0) + h\nu \rightarrow CH_3 + HCO \quad (4)$$
$$CH_3CHO(S_0) + h\nu \rightarrow CH_4 + CO \quad (5)$$

Channels (1) and (2) have only been recently detected at 205 nm [15] and 248 nm [16]. Channel (3) has never

*Authors to whom correspondence should be addressed. E-mail: qunzh@ustc.edu.cn, yangchen@ustc.edu.cn, cshuang@dicp.ac.cn

been observed experimentally. Channels (4) and (5) have been proven to be the dominant decay pathways and account for most of the total quantum yield.

Channel (5), the molecular channel, has been investigated over recent years. In 2001, Gherman and coworkers studied the molecular photodissociation channel of acetaldehyde at 248 nm using the vacuum UV laser induced fluorescence (LIF) method [11]. The product CO molecule is highly rotationally excited but vibrationally not excited and the product CH_4 is vibrationally hot. The dissociation of acetaldehyde occurs on the S_0 surface via a transition state, whose geometry has been determined by *ab initio* quantum chemical calculations [11, 27, 28, 30]. The theoretical results obtained at that time qualitatively agreed with the experimental findings. However, in 2006, Houston and Kable found that there were two kinds of CO fragments, the internal energy distributions of which were different, in the photodissociation of acetaldehyde at 308 nm [14]. Their experimental results included the rotationally hot CO, which is in agreement with the findings of Gherman and coworkers, and the rotationally cold CO, which could not be explained by the transition state mechanism. Similar to the case of formaldehyde [38, 39], the new type of CO fragments was assigned to a roaming dissociation pathway. The later theoretical and experimental results [17, 32, 34] supported the findings.

The roaming mechanism is characterized by large amplitude motion associated with a failed radical dissociation. In acetaldehyde dissociation the initial step is the breaking of the C−C bond to form CH_3 and HCO as forming the radical products. However, both radicals cannot completely escape from each other, instead they "roam" around each other. At some stage in the "roaming" process, the CH_3 encounters the H-atom of HCO and abstracts it from the HCO to produce CH_4 and CO. Since roaming can be thought as an intramolecular abstraction, the CO fragment is rotationally cold and with low translational energy.

Channel (4), the radical channel, has been studied at several different photolysis energies and proven to be the major process for the dissociation of acetaldehyde in the UV region. The photodissociation dynamics of acetaldehyde in the radical channel can be described by two competing dissociation mechanisms. Following excitation to S_1, acetaldehyde dissociates into CH_3 and HCO fragments by intersystem crossing to T_1 or internal conversion back to S_0. The time scale of the intersystem crossing is ∼0.1 ns, the dissociation is slow with respect to rotational period of parent molecule. For the triplet photodissociation, the rotational and vibrational energy distributions of HCO fragment have been investigated at several different wavelengths [3, 4, 6, 13, 29, 31]. Both fragments are formed with large translational energy release and low internal excitation. In the absence of an accurate potential energy surface for the dissociation, the rotational and vibrational energy distributions have been interpreted by statistical [40] and impulsive [41] models. The dissociation on S_0 has been found only in recent years [18, 21]. The fragments are formed with lower translational energy release and high internal excitation. Fu and coworkers [37] reported trajectory surface hopping calculations of the three-state photodissociation of acetaldehyde using full dimensional *ab initio* potential energy surfaces and spin-orbit couplings. Their results indicated that the T_1:S_0 branching ratio to form the radical products CH_3 and HCO from T_1 and S_0 increases with increasing photolysis energy. The height of triplet barrier has been determined by several groups [3, 6, 7, 13, 21]. But the values for the triplet exit barrier reported by different groups are inconsistent. Heazlewood *et al.* estimated a range for the triplet barrier height between 3.895 and 3.838 eV above ground state acetaldehyde [18].

Although the radical channel has been extensively studied, the dynamics and the nascent distributions of both fragments are still insufficient. In the present work, we reinvestigate the photodissociation dynamics of acetaldehyde in the region of 275−321 nm by using the time-sliced velocity map imaging technique. The CH_3 fragment is directly probed using (2+1) REMPI detection. In combination with velocity map imaging, it allows us to probe the CH_3 vibrational state specific dissociation dynamics as well as the state-to-state correlation between HCO and CH_3 (v_2, the umbrella vibration mode of CH_3) in the acetaldehyde photodissociation. At photolysis energy around the triplet barrier, we have re-estimated the height of triplet barrier.

II. EXPERIMENTS

The photodissociation of CH_3CHO at wavelengths between 275 and 321 nm was studied in this work using the time-sliced velocity map imaging technique, which has been described in detail elsewhere [42−45]. In brief, a skimmed molecular beam containing 15%CH_3CHO seeded in 2.5 bar of argon was expanded through a pulsed valve (General valve series 9, 10 Hz repetition rate) with a 0.5 mm orifice. After passing through a 1 mm collimating skimmer, the expansion-cooled CH_3CHO beam was then intersected at 90° by the output of two linearly polarized pulsed dye lasers (dissociation and probe).

The dissociation laser was generated by frequency-doubling of the output from a dye laser (Lambda Physik FL2002) pumped by a XeCl excimer laser (Lambda Physik LPX200), the typical power of ∼0.4 mJ/pulse was focused by a spherical quartz lens with f=300 mm. About 20 ns later, the produced methyl radical fragments were ionized by the probe laser, which was the output of a neodymium-doped yttrium aluminum garnet (Nd: YAG) pumped dye laser (Surelite III plus Radiant, Continuum; typical energy ∼2 mJ/pulse) and focused by an f=300 mm spherical quartz lens. The methyl radical fragments were detected via a (2+1)

DOI:10.1063/1674-0068/27/03/249-255

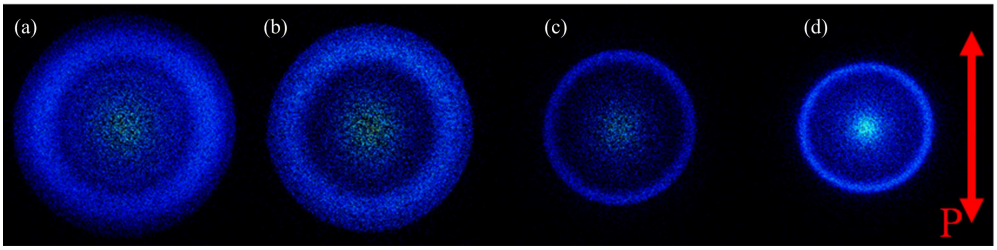

FIG. 2 Slicing images of the CH_3 (v_2=0) products from photodissociation of CH_3CHO at (a) 275 nm, (b) 283 nm, (c) 308 nm and (d) 318 nm.

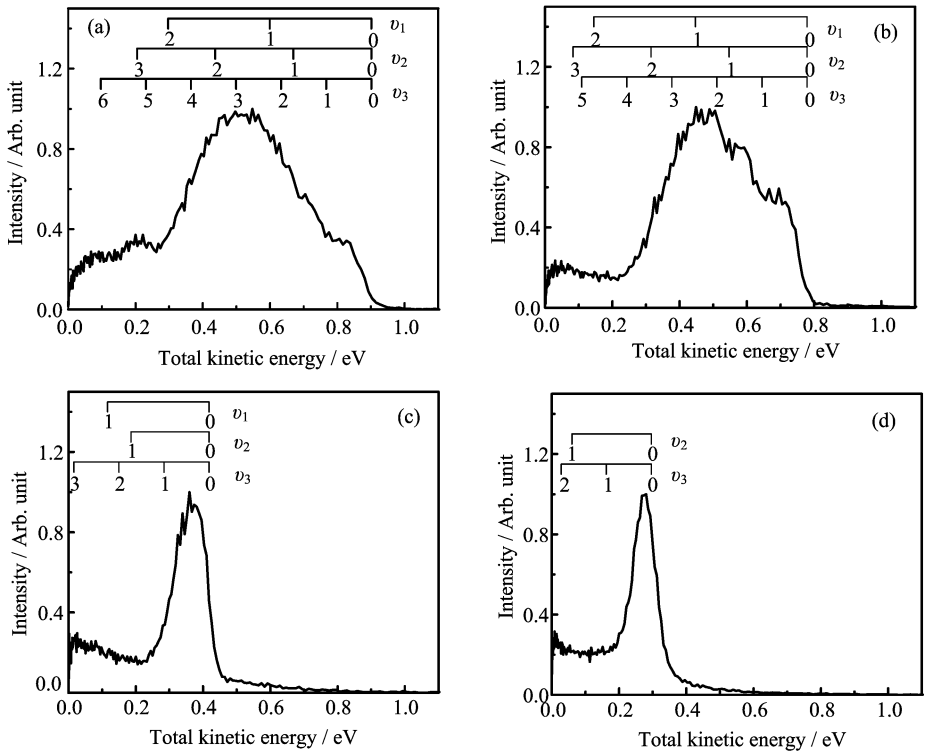

FIG. 3 The product total released kinetic energy distribution from the corresponding images in Fig.2 (a) 275 nm, (b) 283 nm, (c) 308 nm, and (d) 318 nm. v_1: HCO CH-stretch mode, v_2: HCO CO-stretch mode, v_3: HCO bending mode.

REMPI process on the Q branch of $3p(^2A_2'')\leftarrow X(^2A_2'')$ transition. The electric vector of the linearly polarized laser was set perpendicular to the time-of-flight axis and thus parallel to the plane of the detector.

The methyl radical ions were accelerated by the focusing electric fields and projected onto a 40-mm-diameter Chevron multi-channel plates (MCP) coupled to a P-47 phosphor screen (APD 3040FM, Burle Electro-Optics). A fast high-voltage switch (PVM-4210, DEI; typical duration ~80 ns) was pulsed to gate the gain of the MCP's for mass selection as well as the time slicing of the ion packets. The transient images from the phosphor screen were captured by a cooled charge-coupled device (CCD) camera (ImagerPro2 M 640×480 pixels, LaVision) and transferred to a computer on an every shot basis for event counting [46] and data analysis. Meanwhile, the fluorescence from the phosphor screen was monitored with a photomultiplier tube to optimize the experimental conditions and scan the REMPI spectrum. Timing of the pulsed valve, dissociation and ionization lasers, and the gate pulse applied to the MCP's was controlled by a multichannel digital delay pulse generator (BNC Model 555).

III. RESULTS

Figure 2 shows the slicing images of the CH_3 products (v_2=0) from photodissociation of CH_3CHO at 275, 283, 308 and 318 nm when the probe laser is tuned to Q branch of the $3p(^2A_2'')\leftarrow X(^2A_2'')$ transition of CH_3 fragment. The total translational energy distributions in the center-of-mass frame for the CH_3 products are extracted from Fig.2, and the results are shown in Fig.3. As can be seen in Fig.3, the translational energy distri-

DOI:10.1063/1674-0068/27/03/249-255

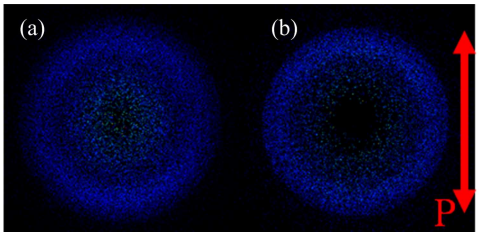

FIG. 4 Slicing images of the CH_3 (v_2=1) products from photodissociation of CH_3CHO at (a) 275 nm and (b) 283 nm.

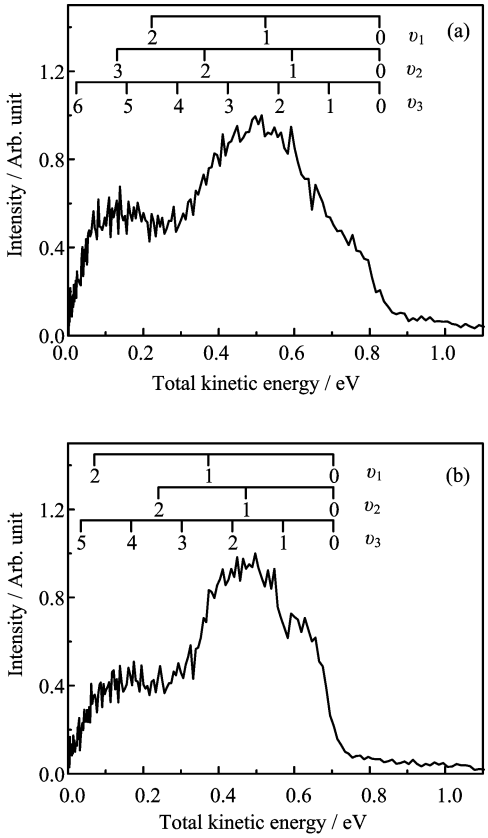

FIG. 5 The product total released kinetic energy distribution from the corresponding images in Fig.4 (a) 275 nm and (b) 283 nm.

butions exhibit bimodal feature: a weak feature in the low energy region and a strong peak in the high energy region. Such feature has also been found in the study of the photodissociation of acetaldehyde at wavelengths between 315 and 325 nm by Amaral *et al.* [21], and they concluded that it arose from two different dissociation mechanisms: the high kinetic energy component comes from dissociation on T_1 after intersystem crossing from S_1, while the low kinetic energy component comes from dissociation on S_0 after internal conversion from S_1. As for our experiment, the background generated by probe laser appears in the low kinetic energy region, so we couldn't consider this region here. The high energy component, which is in agreement with the

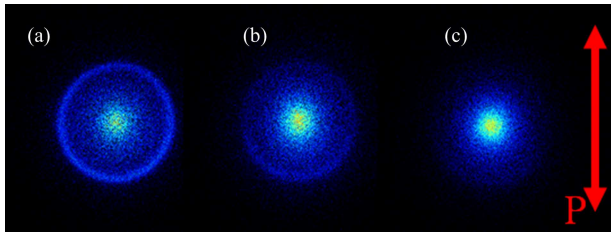

FIG. 6 Slicing images of the CH_3 (v_2=0) products from photodissociation of CH_3CHO at (a) 319 nm, (b) 320 nm, and (c) 321 nm.

results of Amaral and coworkers, comes from dissociation on T_1 state. In the following, we mainly discuss about dissociation on T_1 state.

Due to (2+1) REMPI detection, the internal energy of CH_3 is fixed, the product total translational energy distributions correspond to the internal energy distributions of HCO. As shown in Fig.3, the HCO internal energy increases dramatically from 318 nm to 275 nm. At 318 nm, it is just above the T_1 barrier, the HCO fragment is formed with little vibrational excitation, and cold rotational distribution. At the shorter wavelength 308 nm, the HCO fragment is also formed with little vibrational excitation, but the rotational excitation increases. At 283 and 275 nm with a further increase in excitation energy, the HCO is formed with vibrational excitation and broader internal energy distribution and the HCO vibrational distributions are inverted. Kono *et al.* also observed the vibrationally excited HCO radicals and identified that the threshold wavelengths for the bending and CO-stretching excitations were 308.7 and 302.6 nm [47].

And we detect the vibrationally excited CH_3 fragment at 275 and 283 nm. Figure 4 shows the slicing images of the CH_3 (v_2=1) products from photodissociation of CH_3CHO at 275 and 283 nm. The corresponding total translational energy distributions obtained from the raw images are shown in Fig.5. As can be seen in Fig.5, the HCO is also formed with vibrational excitation and broad internal energy distribution. And the HCO vibrational distributions are also inverted. The HCO internal energy corresponding to the CH_3 umbrella mode excited state (v_2=1) also increases as the photodissociation energy increases.

At the same photolysis energy, for instance, at 283 nm, the HCO vibrational distributions corresponding to different CH_3 umbrella mode excited states are obviously different. The HCO vibrational peak for the CH_3 ground state is at v_3=2, as shown in Fig.3(b). While the HCO vibrational peak for the CH_3 vibrationally excited state is at v_3=1, as seen in Fig.5(b). The vibrational excitation of HCO obviously decreases as the CH_3 umbrella mode excitation increases.

However, at longer wavelengths (around 320 nm), which correspond to excitation energies around the triplet barrier, we observe a sudden change in the to-

DOI:10.1063/1674-0068/27/03/249-255

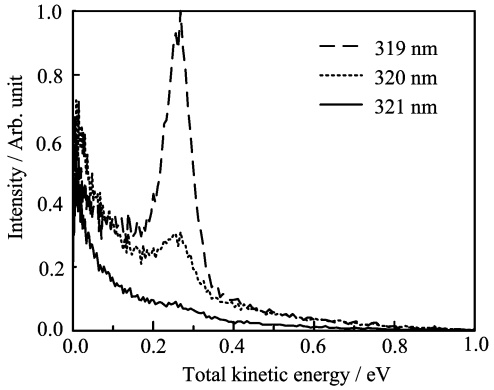

FIG. 7 The product total released kinetic energy distribution from the corresponding images in Fig.6 at 319, 320, and 321 nm.

tal translational energy distributions. Figure 6 displays the slicing images of the CH_3 (v_2=0) products from photodissociation of CH_3CHO at 319, 320 and 321 nm. The total kinetic energy distributions are described from the images directly as shown in Fig.7. At 319 nm, there is an intense ring at the high energy region, which corresponds to dissociation on T_1 after intersystem crossing from S_1. As the excitation energy decreases, the intensity of the ring at the high energy region is reduced obviously at 320 nm. While at 321 nm (a longer photolysis wavelength), the ring completely disappears. Only one component exists in the low energy region.

IV. DISCUSSION

There are a number of energetically allowed channels involved in the photodissociation of CH_3CHO. In our experiments, we are concerned with the radical channel leading to CH_3+HCO. Following excitation to S_1, CH_3CHO intersystem crosses to T_1, where the products can be directly formed after exceeding a barrier on T_1, or goes back to S_0 by internal conversion and then dissociates into the fragments. For CH_3CHO dissociation on T_1 after intersystem crossing from S_1, the products are formed with high fragment kinetic energy and low internal energy distributions. The internal energy of both fragments increases as the photolysis energy increases. A lot of experimental and theoretical studies [3, 4, 6, 13, 28, 29, 47] focus on the triplet photodissociation pathway. As mentioned above, the product total kinetic energy distributions correspond to the internal energy distributions of HCO. So it can be seen from Fig.3 that the distributions among rotational states of product HCO are increased and widened with increased photodissociation energy. The results are consistent with the findings of Lee *et al.* [6] and Cruse *et al.* [13]. The results of Lee and co-workers indicated that the populations of rotational states of HCO displayed a Gaussian-type distribution. Cruse and co-workers found that the rotational distributions of both fragments increase with photolysis energy, with a lesser degree of excitation in the CH_3 fragment.

Interestingly, at photodissociation energy just above the T_1 barrier, although the energy released after the T_1 barrier is sufficient for the vibrational excitations of fragments, we could not observe the vibrationally excited fragments. Kono *et al.* [47] and Cruse *et al.* [13] also found this phenomenon. Kono *et al.* suggested that after dissociation of CH_3CHO the excess energy released below the barrier is mainly partitioned into rotation and translation of fragments and the vibrational excitation of fragments is solely determined by the excess energy above the barrier top [47]. Terentis and coworkers [4] suggested that the low vibrational energy distributions of fragments would be consistent with the impulsive model. Exceeding the barrier to dissociation on the triplet state occurs late (C−C bond length of 2.13 Å). The late barrier inhibits coupling of the excess energy into vibrational energy of fragments. Therefore, the fragments are vibrational cold.

However, at higher photolysis energy (283 and 275 nm), the internal energy distributions of products are significantly widened and the vibrational excitation fragments are observed, as shown in Fig.3 (a) and (b). Furthermore, the HCO vibrational distributions are inverted. As can be seen, the degree of HCO vibrational excitation increases with photolysis energy. And the umbrella mode excited state of CH_3 is directly detected for the first time using the velocity map imaging technique, as seen in Fig.4. Cruse and coworkers suggested that preferential excitation of the umbrella mode of CH_3 is expected as a result of the "flattening" of the methyl group on dissociation [13]. Yadav *et al.* [23] and Kurosaki *et al.* [28] reported the transition state structure of acetaldehyde at the top of the barrier on the T_1 potential energy surface using *ab initio* calculations. When the elongated C−C bond is broken, the repulsive force is along the direction of the methyl symmetry axis, resulting in the umbrella mode excitation of CH_3 fragment. For the umbrella mode excited CH_3, the corresponding HCO fragment is also vibrationally excited and the HCO vibrational distributions are also inverted (Fig.5). And the degree of HCO vibrational excitation also increases as the photodissociation energy increases. At the same photolysis energy, the HCO vibrational distributions corresponding to different CH_3 umbrella mode excited states are obviously different. The results indicate that there is a clear vibrational state-to-state correlation between the HCO and CH_3 fragments.

In the previous study of acetaldehyde photodissociation, the height of triplet barrier has been controversial [3, 6, 7, 13, 21]. In a recent study, using the velocity-map imaging technique, Amaral *et al.* determined the triplet exit barrier of 3.893±0.006 eV above the ground state of acetaldehyde [21]. However, in the same way, we find that the height of triplet barrier is lower than their results. Figures 6 and 7 show this result. At 319

DOI:10.1063/1674-0068/27/03/249-255

nm, the excitation energy is above the T_1 barrier, the observed signals in high kinetic energy region indicate that the triplet photodissociation pathway is opened. At 321 nm, the disappearance of the fast component indicates that the triplet photodissociation pathway is closed. At 320 nm, the results are similar to the findings of Amaral *et al.* at 319 nm. The fast component is still present, but its intensity is significantly weakened. The much less fast component can be interpreted as the results of vibrationally excited parent acetaldehyde dissociation above the triple barrier. Therefore, the triplet barrier can be determined between 319 and 320 nm. We estimate a value of 3.881±0.006 eV above ground state acetaldehyde, which is slightly less than the results of Amaral *et al.*

V. CONCLUSION

Using time-sliced velocity map imaging technique, the photodissociation dynamics of CH_3CHO at wavelengths between 275 and 321 nm for the radical channel leading to CH_3+HCO has been reinvestigated. Two photodissociation pathways participate in the dissociation process together. Following excitation to S_1, acetaldehyde dissociates into CH_3 and HCO fragments by intersystem crossing to T_1 or internal conversion back to S_0. We mainly discuss dissociation on T_1 state. For the pathway dissociation on T_1 after intersystem crossing from S_1, the products are formed with high translational energy and low internal energy. The rotational and vibrational energy distributions of both fragments increase with photodissociation energy. The HCO and CH_3 fragments are vibrational state-to-state correlated. The height of triplet barrier is estimated at 3.881±0.006 eV above ground state acetaldehyde.

VI. ACKNOWLEDGMENTS

This work was supported by the National Natural Science Foundation of China (No.21203186 and No.21073187), the National Key Basic Research Program of China (No.2010CB923302), 100 Talents Program of Chinese Academy of Sciences, and Knowledge Innovation Program of Chinese Academy of Sciences.

[1] A. Horowitz, C. J. Kerchner, and J. G. Calvert, J. Phys. Chem. **86**, 3094 (1982).
[2] A. Horowitz and J. G. Calvert, J. Phys. Chem. **86**, 3105 (1982).
[3] T. Kono, M. Takayanagi, and I. Hanazaki, J. Phys. Chem. **97**, 12793 (1993).
[4] A. C. Terentis, M. Stone, and S. H. Kable, J. Phys. Chem. **98**, 10802 (1994).
[5] J. M. Price, J. A. Mack, G. Helden, X. Yang, and A. M. Wodtke, J. Phys. Chem. **98**, 1791 (1994).
[6] S. H. Lee and I. C. Chen, J. Chem. Phys. **105**, 4597 (1996).
[7] T. Gejo, H. Bitto, and J. R. Huber, Chem. Phys. Lett. **261**, 443 (1996).
[8] H. Liu, E. C. Lim, C. Muñoz-Caro, A. Niño, R. H. Judge, and D. C. Moule, J. Chem. Phys. **105**, 2547 (1996).
[9] S. H. Lee and I. C. Chen, Chem. Phys. **220**, 175 (1997).
[10] G. H. Leu, C. L. Huang, S. H. Lee, Y. C. Lee, and I. C. Chen, J. Chem. Phys. **109**, 9340 (1998).
[11] B. F. Gherman, R. A. Friesner, T. H. Wong, Z. Min, and R. Bersohn, J. Chem. Phys. **114**, 6128 (2001).
[12] J. R. Huber, Chem. Phys. Lett. **377**, 481 (2003).
[13] H. A. Cruse and T. P. Softley, J. Chem. Phys. **122**, 124303 (2005).
[14] P. L. Houston and S. H. Kable, Proc. Natl. Acad. Sci. USA **103**, 16079 (2006).
[15] T. Y. Kang, S. W. Kang, and H. L. Kim, Chem. Phys. Lett. **434**, 6 (2007).
[16] L. Rubio-Lago, G. A. Amaral, A. Arregui, J. G. Izquierdo, F. Wang, D. Zaouris, T. N. Kitsopoulos, and L. Bañares, Phys. Chem. Chem. Phys. **9**, 6123 (2007).
[17] B. R. Heazlewood, M. J. T. Jordan, S. H. Kable, T. M. Selby, D. L. Osborn, B. C. Shepler, B. J. Braams, and J. M. Bowman, Proc. Natl. Acad. Sci. USA **105**, 12719 (2008).
[18] B. R. Heazlewood, S. J. Rowling, A. T. Maccarone, M. J. T. Jordan, and S. H. Kable, J. Chem. Phys. **130**, 054310 (2009).
[19] S. H. Lee, J. Chem. Phys. **131**, 174312 (2009).
[20] R. Sivaramakrishnan, J. V. Michael, and S. J. Klippenstein, J. Phys. Chem. A **114**, 755 (2010).
[21] G. A. Amaral, A. Arregui, L. Rubio-Lago, J. D. Rodriguez, and L. Banares, J. Chem. Phys. **133**, 064303 (2010).
[22] L. Rubio-Lago, G. A. Amaral, A. Arregui, J. Gonzalez-Vazquez, and L. Banares, Phys. Chem. Chem. Phys. **14**, 6067 (2012).
[23] J. S. Yadav and J. D. Goddard, J. Chem. Phys. **84**, 2682 (1986).
[24] H. Tachikawa and N. Ohta, Chem. Phys. Lett. **224**, 465 (1994).
[25] O. Setokuchi, S. Matuzawa, and Y. Shimizu, Chem. Phys. Lett. **284**, 19 (1998).
[26] R. A. King, W. D. Allen, and H. F. Schaefer III, J. Chem. Phys. **112**, 5585 (2000).
[27] Y. Kurosaki and K. Yokohama, J. Phys. Chem. A **106**, 11415 (2002).
[28] Y. Kurosaki and K. Yokohama, Chem. Phys. Lett. **371**, 568 (2003).
[29] M. N. D. S. Cordeiro, E. Martínez-Núñez, A. Fernández-Ramos, and S. A. Vázquez, Chem. Phys. Lett. **375**, 591 (2003).
[30] Y. Kurosaki, Chem. Phys. Lett. **421**, 549 (2006).
[31] K. C. Thompson, D. L. Crittenden, S. H. Kable, and M. J. T. Jordan, J. Chem. Phys. **124**, 044302 (2006).
[32] B. S. Shepler, B. J. Braams, and J. M. Bowman, J. Phys. Chem. A **111**, 8282 (2007).
[33] Y. Kurosaki, J. Mol. Struct.: THEOCHEM **850**, 9 (2008).
[34] B. C. Shepler, B. J. Braams, and J. M. Bowman, J.

DOI:10.1063/1674-0068/27/03/249-255

Phys. Chem. A **112**, 9344 (2008).
[35] S. Chen and W. H. Fang, J. Chem. Phys. **131**, 054306 (2009).
[36] L. B. Harding, Y. Georgievskii, and S. J. Klippenstein, J. Phys. Chem. A **114**, 765 (2010).
[37] B. N. Fu, Y. C. Han, and J. M. Bowman, Faraday Discuss. **157**, 27 (2012)
[38] R. D. van Zee, M. F. Foltz, and C. B. Moore, J. Chem. Phys. **99**, 1664 (1993).
[39] D. Townsend, S. A. Lahankar, S. K. Lee, S. D. Chambreau, A. G. Suits, X. Zhang, J. Rheinecker, L. B. Harding, and J. M. Bowman, Science **306**, 1158 (2004).
[40] E. Zamir and R. D. Levine, Chem. Phys. **52**, 253 (1980).
[41] G. E. Busch and K. R. Wilson, J. Chem. Phys. **56**, 3626 (1972).
[42] C. S. Huang, C. M. Zhang, and X. M. Yang, J. Chem. Phys. **132**, 154306 (2010).
[43] C. M. Zhang, J. L. Li, Q. Zhang, Y. Chen, C. S. Huang, and X. M. Yang, Phys. Chem. Chem. Phys. **14**, 2468 (2012).
[44] J. L. Li, C. M. Zhang, Q. Zhang, Y. Chen, C. S. Huang, and X. M. Yang, J. Chem. Phys. **134**, 114309 (2011).
[45] Z. C. Chen, Q. Shuai, A. T. J. B. Eppink, B. Jiang, D. X. Dai, X. M. Yang, and D. H. Parker, Phys. Chem. Chem. Phys. **13**, 8531 (2011).
[46] B. Y. Chang, R. C. Hoetzlein, J. A. Mueller, J. D. Geiser, and P. L. Houston, Rev. Sci. Instrum. **69**, 1665 (1998).
[47] T. Gejo, M. Takayanagi, T. Kono, and I. Hanazaki, Chem. Phys. Lett. **218**, 343 (1994).

DOI:10.1063/1674-0068/27/03/249-255